Microwave photonic filter with a continuously tunable central frequency using an SOI high-Q microdisk resonator*

Liu Li(刘 力), Yang Ting(杨 婷), and Dong Jian-Ji(董建绩)†

Wuhan National Laboratory for Optoelectronics, School of Optoelectronic Science and Engineering, Huazhong University of Science and Technology, Wuhan 430074, *China*

(Received 4 November 2013; revised manuscript received 15 March 2014; published online 24 July 2014)

Utilizing a high-Q microdisk resonator (MDR) on a single silicon-on-insulator (SOI) chip, a compact microwave photonic filter (MPF) with a continuously tunable central frequency is proposed and experimentally demonstrated. Assisted by the optical single side-band (OSSB) modulation, the optical frequency response of the MDR is mapped to the microwave frequency response to form an MPF with a continuously tunable central frequency and a narrow 3-dB bandwidth. In the experiment, using an MDR with a compact size of 20×20 μm^2 and a high Q factor of 1.07×10^5, we obtain a compact MPF with a high rejection ratio of about 40 dB, a 3-dB bandwidth of about 2 GHz, and a frequency tuning range larger than 12 GHz. Our approach may allow the implementation of very compact, low-cost, low-consumption, and integrated notch MPF in a silicon chip.

Keywords: microwave photonic filter (MPF), microdisk resonator (MDR), silicon-on-insulator (SOI) chip, optical single side-band (OSSB) modulation

PACS: 32.30.Bv, 84.40.–x, 42.79.Ci **DOI:** 10.1088/1674-1056/23/9/093201

1. Introduction

Optical technology can be used to improve the performance of microwave and millimeter-wave systems due to its huge bandwidth, electromagnetic immunity, low loss, and light weight.[1] Among the photonic microwave signal processing functionalities, microwave photonic filter (MPF) is of particular interest since it can provide large bandwidth with flexible tunability, which is difficult to realize by conventional electronic methods. To date, different MPF schemes have been proposed.[2–6] In particular, the notch MPF can play a critical role in microwave photonic systems to enable the blocking of undesired spectral contents and signal monitoring.[7] The notch MPFs with high quality have been previously demonstrated using differential fiber delays,[8] Bragg gratings,[9] cascaded microring resonators (CMRRs),[10] and high-birefringence fiber-based optical components.[11,12] Compared to these fiber optic systems, silicon-based waveguides can offer distinct advantages of increased stability, reliability, compactness, and capability of integration with electronics.[7,13] In recent years, some MPFs based on silicon microring resonators (MRRs) and microdisk resonators (MDRs) have been presented, indicating excellent characteristics of reconfigurability[14] or bandwidth tenability,[15–17] but the design and fabrication of the devices are a little complex and difficult. In addition, to achieve the high-Q MPF with a good frequency selectivity, one expects to seek some integrated optical filters with a very narrow bandwidth, such as a high-Q MDR.[18] A detailed research of ultra-high-Q MDR has been presented.[19]

In this paper, we demonstrate a compact notch MPF based on a silicon-on-insulator (SOI) MDR with a radius of 10 μm. With a optical single sideband (OSSB) modulation, the central operating frequency of the notch MPF can be continuously tuned by slightly shifting the optical carrier at the edge of the MDR resonance frequencies. The narrow bandwidth of the MPF is 2 GHz, and the Q factor is higher than our previous scheme.[10] The silicon waveguides in our scheme is easily fabricated without thermal nodes or electrode auxiliary.

2. Operation principle

The notch MPF is based on an SOI microdisk resonator which consists of a single bus waveguide and a laterally coupled disk. According to the coupling mode and transfer matrix theories, transmission spectrum of the through port of the MDR is a periodical notch filter. We assume that a random radio frequency (RF) signal is modulated onto an optical carrier by the OSSB, and define the frequency of the optical carrier and the sideband as f_0 and f_0+f_1, respectively. Then the OSSB signal (f_0 and f_0+f_1) is launched into the high-Q MDR. The optical carrier (f_0) is well adjusted to locate around the edge of one resonance frequency (see Fig. 1(a)). When the sideband component (f_0+f_1) is just aligned with the notch frequency, the output RF response should be null due to the absence of a beat frequency, otherwise the RF response reaches

*Project supported by the National Basic Research Program of China (Grant No. 2011CB301704), the Program for New Century Excellent Talents in Ministry of Education of China (Grant No. NCET-11-0168), the Foundation for the Author of National Excellent Doctoral Dissertation of China (Grant No. 201139), and the National Natural Science Foundation of China (Grant Nos. 60901006 and 11174096).

†Corresponding author. E-mail: jjdong@mail.hust.edu.cn

© 2014 Chinese Physical Society and IOP Publishing Ltd

the maximum. Therefore, the output RF response is a notch MPF. If the optical carrier is slightly shifted with an interval of f_1, f_2, and f_3 to the notch frequency, the central frequency of the notch MPF can also be tuned according to the above three frequency offsets (see Fig. 1(b)). Since the optical carrier can be tuned continuously, our MPF is capable of tuning the central frequency continuously, which is not possible in our previous scheme.[8] In addition, the frequency tunability can be achieved by changing the optical carrier rather than the resonant frequency of the silicon waveguides. Furthermore, the silicon waveguides in our scheme can be easily fabricated without thermal nodes or electrode auxiliary.

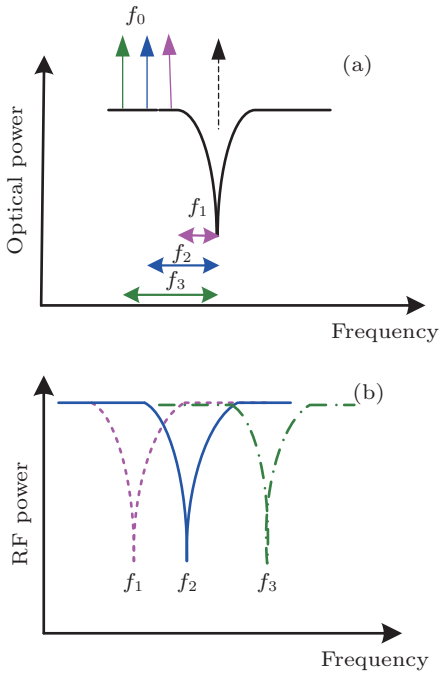


Fig. 1. (color online) Tunability of central frequency. (a) MDR and (b) RF spectrum of MPF.

The MDR is fabricated on the SOI wafer. We use a finite-element mode solver (COMSOL Multiphysics) to optimize the waveguide performance. In order to reduce the transmission loss of the waveguide, we design a structure of ridge waveguide on the SOI wafer. The width of the straight bus waveguide is 500 nm. The silicon shallow layer and deep layer have the thicknesses of 100 nm and 240 nm, respectively. To optimize the MDR, figure 2(a) illustrates the effective mode indices for different radial modes of the MDR with a radius of 10 μm. It can be seen that, the 2nd-order radial mode has an effective index which is closer to the straight WG. Hence, this 2nd-order mode has a better phase matching with the waveguide mode, thereby resulting in a stronger coupling and a lower Q factor. Table 1 shows the Q factors of the MDR at different gap parameters (gap between the bus WG and the disk). In terms of the MDR, the 2nd-order radial mode has a lower Q factor than the fundamental mode. Optimizing both the Q factor and the extinction ratio (ER), the final best gap for the MDR is about 350 nm. Figure 2(b) also shows the mode distributions of the cross section of the ridge MDR on the oxide substrate. It is obvious that the majority of all radial modes is confined at the center of the waveguides.

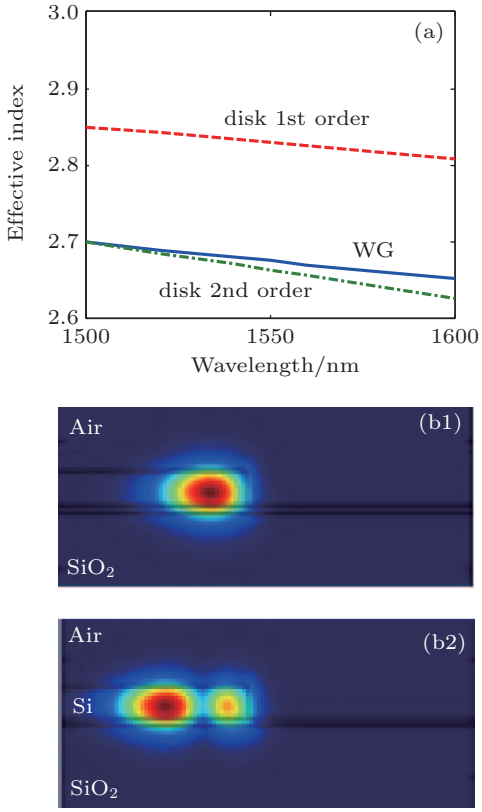


Fig. 2. (color online) Simulated results using the COMSOL software. (a) Effective indices of different modes of MDR and the straight waveguide (WG); the energy profile of the fundamental mode (b1) and 2nd-order mode (b2) of MDR.

Table 1. The Q factors of the MDR at different gap parameters.

Gap/nm	$Q^{a)}/10^4$	$Q^{b)}/10^4$
250	24.7	16.8
300	35.3	23.6
350	56.2	29.8

[a)]Fundamental radial mode of the MDR, [b)]2nd-order radial mode of the MDR.

To pursue a high-Q MPF, the employed silicon resonators should also have a high Q factor. For this purpose, we fabricate several MDRs on the corresponding commercial SOI wafers to attain the highest Q factor. Figure 3(a) shows the scanning electron microscope (SEM) images of the fabricated MDR with a radius of 10 μm. The thickness of the top silicon layer of the SOI wafers is 340 nm and the thickness of the buried oxide layer is 2 μm. The device pattern was transferred to a photoresist (ZEP520A) by the E-beam lithography (Vistec EBPG5000+ES). The upper silicon layer was then etched downward for 240 nm to form a ridge waveguide through the

induced coupled plasma (ICP) etching (Oxford Instruments Plasmalab System100). For the MDR of the highest Q factor, the bus waveguide has a width of 500 nm, and the gap is about 350 nm. The zoom-in coupling region is shown in Fig. 3(b). We employ the vertical grating coupler to couple the optical signal from fiber to silicon waveguide, and the zoom-in grating coupler is shown in Fig. 3(c). The grating couplers have a period of 630 nm, and the duty cycle is 56%. The coupling loss of the grating couplers is measured to be 5 dB for a single side.

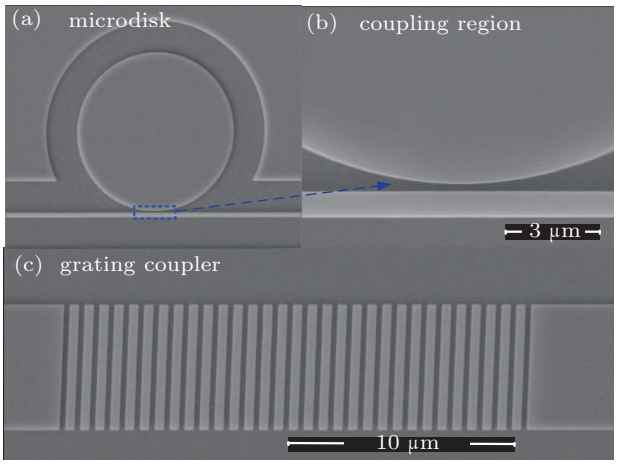


Fig. 3. (a) SEM images of the MDR, (b) coupling region between the straight waveguide and the bending MDR waveguide, and (c) the grating coupler.

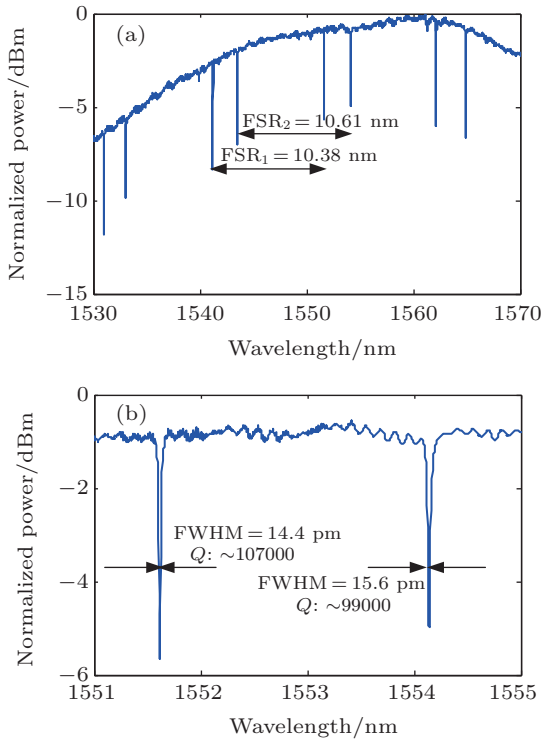


Fig. 4. (color online) (a) Measured spectrum of the MDR and (b) its zoom in high-Q spectrum.

Specific testing method is to inject a transverse electric (TE) polarized light into the device and measure the transmission spectrum by using a swept-wavelength test setup (see Fig. 4(a)). There are two periodic bandstop filters with different FSRs (FSR$_1$ = 10.38 nm and FSR$_2$ = 10.61 nm) at the through port. This means that only two radial modes are effectively excited. Figure 4(b) shows the zoom-in resonance notch with the highest Q factor of 1.07×10^5.

The frequency response of the notch MPF can also be deduced analytically. Assume that the optical carrier is modulated in a phase modulator (PM) by the RF signal. In the case of phase modulation, the output optical field of the PM can be described by

$$E_{\text{out}}(t) = E_0\,\mathrm{e}^{\mathrm{j}[\omega_0 t+\gamma\cos(\omega_{\text{RF}}t)]}, \tag{1}$$

where E_0 is amplitude of the input optical field, ω_0 is the angular frequency of the input optical signal, ω_{RF} is angular frequency of the RF signal, and γ is the phase modulation depth. Neglecting the high-order side-band, the output optical field of the PM under a small signal model can be described by

$$\begin{aligned} E_{\text{out}}(t) \;=\; & \sqrt{P_0}[\mathrm{j}\mathrm{J}_1(\gamma)\,\mathrm{e}^{\mathrm{j}(\omega_0-\omega_{\text{RF}})t} \\ & +\mathrm{J}_0(\gamma)\,\mathrm{e}^{\mathrm{j}\omega_0 t}+\mathrm{j}\mathrm{J}_1(\gamma)\,\mathrm{e}^{\mathrm{j}(\omega_0+\omega_{\text{RF}})t}], \end{aligned} \tag{2}$$

where P_0 is the optical power, expressed by $P_0 = |E_0|^2$, and $\mathrm{J}_n(\gamma)$ $(n = 0, 1)$ is the nth-order Bessel function of the first kind. We then use a rectangular bandpass filter to eliminate one sideband (ω_0–ω_{RF}). After the signal is transmitted in the MDR with an amplitude transmission function of $H(\omega)$, each frequency component will multiply a different frequency weight of $H(\omega)$, so the output optical field can be described as

$$E(\omega) = 2\pi\sqrt{P_0}[\mathrm{J}_0(\gamma)H(\omega_0)+\mathrm{j}\mathrm{J}_1(\gamma)H(\omega_0+\omega_{\text{RF}})]. \tag{3}$$

After detecting the square-law photo-detector (PD), and neglecting the J_1^2 term, we obtain the alternative current (AC) term of the current as

$$i_{\text{AC}} \propto 4\pi^2\mathrm{j}P_0\mathrm{J}_0(\gamma)\mathrm{J}_1(\gamma)H^*(\omega_0)H(\omega_0+\omega_{\text{RF}}). \tag{4}$$

From Eq. (4), we can see that if the first-order sideband component is aligned at the notches of the MDR, the response of the microwave photonic filter is a null, otherwise it is a constant. Therefore, a notch MPF can be obtained. Since the optical carrier is at the edge of the notches (see Fig. 1), $H(\omega_0)$ is nearly a constant. Hence, the MPF frequency response is mainly determined by the response of the first-order sideband $H(\omega_0+\omega_{\text{RF}})$. This proves that the Q factor of the MPF is positively correlated to the Q factor of the resonance notch of the silicon waveguides.

Utilizing the measured spectra of the MDR (see Fig. 4), we numerically study the notch MPF response by substituting this measured spectrum to Eq. (4). Figure 5 demonstrates the notch MPF response when the laser wavelength is located at the edge of the MDR's resonance wavelength with the highest

Q factor of 1.07×10^5. In order to illustrate the tunability of the central frequency, we select three different laser wavelengths with frequency intervals of 5 GHz, 10 GHz, and 15 GHz to the resonance frequency, respectively. Thus, the final notch frequencies of the MPF are 5 GHz, 10 GHz, and 15 GHz (see Fig. 5).

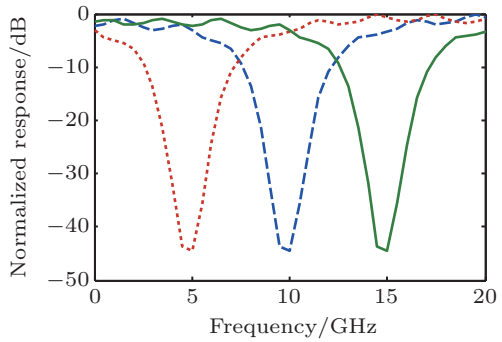


Fig. 5. (color online) Simulated MPF frequency response with tunable central frequency.

3. Experimental results

In order to verify the theoretical analysis and the simulation results, we carry out experiments with the configuration shown in Fig. 6. A tunable laser diode (TLD) emits a continuous wave (CW) beam, which has a precisely tuning resolution of 1 pm. The vector network analyzer (VNA) (Anritsu MS2028C) has a maximum sweeping frequency of 20 GHz. An electrical amplifier (EA) is used to amplify the RF signal from the VNA. The CW beam is modulated by a PM to produce an optical double sideband signal. A forward erbium doped fiber amplifier (EDFA) is used to amplify the input optical power. The tunable optical filter is then used to eliminate one of the first-order sidebands, so an OSSB signal is thus generated and then launched to the silicon waveguide. A polarization controller (PC) is required since the silicon waveguide operates only in a transverse electrical (TE) mode. The vertical grating coupler is used with a 3-dB coupling bandwidth of about 30 nm in the C band. A backward EDFA is used to compensate for the power attenuation by the chip loss. After amplification by the backward EDFA, the optical signal is converted to electrical signal by the PD and analyzed by the VNA. The PD has a bandwidth of 40 GHz.

The PM is used to generate optical double sideband modulation, which can also be replaced by an intensity modulator. It is known that the use of a PM would provide better performance due to its low insertion loss and bias-drift-free

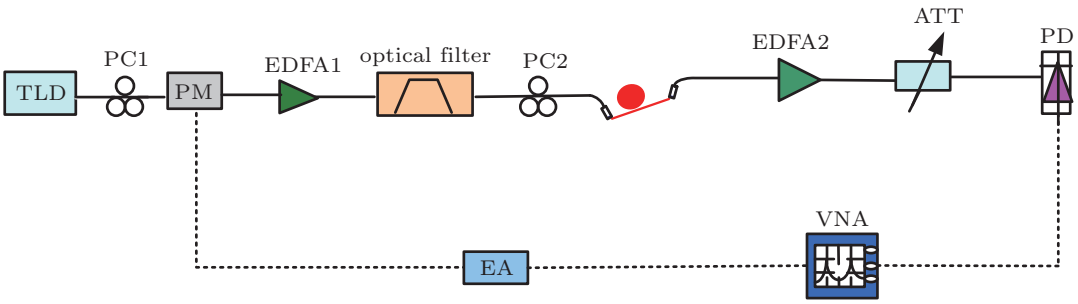


Fig. 6. (color online) Experimental setup of the proposed scheme. Solid lines: optical path, dash lines: electrical path, TLD: tunable laser diode, PC: polarization controller, PM: phase modulator, EDFA: erbium doped fiber amplifier, ATT: attenuator, PD: photodetector, EA: electrical amplifier, and VNA: vector network analyzer.

operation. Figure 7 shows the spectrum of the OSSB modulation. For example, if an RF signal at 19.5 GHz is applied to the PM, one can observe the optical double sideband (ODSB) modulation at the PM output port (red line in Fig. 7). Subsequently, a tunable optical filter is used to remove one sideband. The transmission response of the optical filter is also shown as the dash line. In order to achieve better performance of the beat frequency, the optical carrier is located at the rising edge of the optical filter. Thus, the OSSB modulation is achieved (blue line in Fig. 7). The power of the optical carrier and positive sideband is almost the same. The bandwidth of the OSSB modulator is mainly determined by the spectral characteristics of the optical filter.

Figure 8 illustrates the notch MPF response when using the high-Q MDR. By slightly shifting the laser wavelength around the edge of the resonance wavelength, we can achieve the notch MPF whose central frequency can be tunable. Based

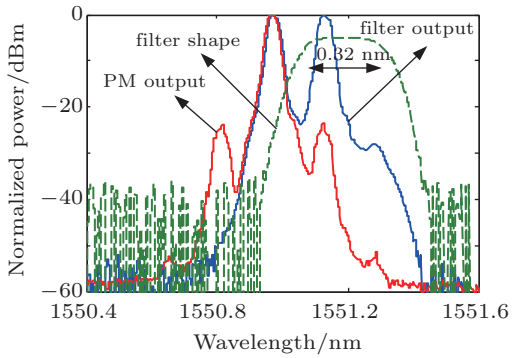


Fig. 7. (color online) Optical single-sideband signal generation using an optical bandpass filter. Dash line: the transmission spectrum of the optical filter; red line: the optical spectrum of the ODSB signal; and blue line: the optical spectrum of generated OSSB signal.

on the above analysis, the high-Q MDR would result in a high-Q MPF, so the narrow 3-dB bandwidth and the maximum Q value of the notch MPF is about 2 GHz and 9, as shown in Fig. 8.

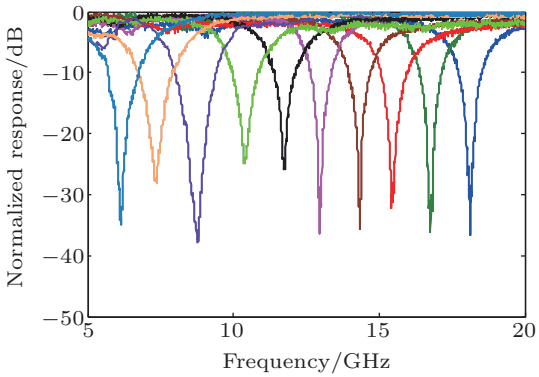


Fig. 8. (color online) Experimental MPF response of the tunable central frequency by using the high-Q MDR.

In order to verify the stability of the central frequency, we also measured the filter responses for four different central frequencies after fifteen minutes. Figure 9 illustrates the comparison of the filter response at the beginning with that after fifteen minutes. The maximum shift of the central frequency is about 30 MHz, which is negligible compared with the tunable range of the central frequency (12 GHz). The change in the ambient temperature may cause the optical spectrum shift of the microdisk resonator, so the stability of the central frequency mainly depends on the ambient temperature. Thus, if the ambient temperature can be controlled accurately, the performance of the MPF will be stable enough.

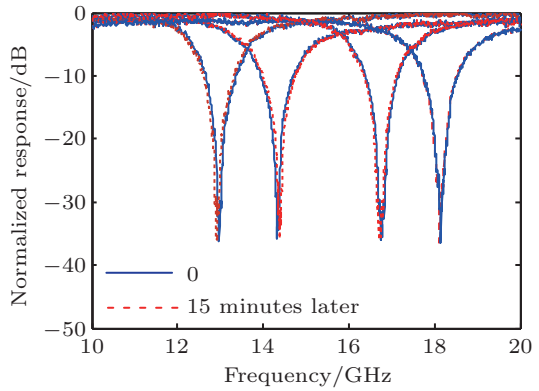


Fig. 9. (color online) Comparison of the filter responses at the beginning and fifteen minutes later.

In the future, we can optimize the chip fabrication process to improve the performance of our MPF system, especially by employing the process of thermal oxidation to reduce the waveguide surface roughness, which can increase the Q factor of the MDR. Through these methods, the power consumption of the system could be further reduced, and the Q factor of the MPF is improved.

4. Conclusion

We have demonstrated compact notch MPFs based on the silicon waveguides of an MDR with the OSSB modulation. The central operating frequencies of the MPFs can be easily tuned by slightly shifting the laser wavelength at the edge of resonance wavelengths. In the experiment, we obtain a high-Q MPF with a high rejection ratio of around 40 dB, 3-dB bandwidth of about 2 GHz, and a frequency tuning range larger than 12 GHz, using a high-Q MDR. Our experiment offers a low-cost, high-Q, and small-size integrated MPF scheme, which can be potentially used for optical monitoring or to reject certain undesired RF bands in microwave photonic systems.

References

[1] Yao J P 2009 *IEEE J. Lightw. Technol.* **27** 314
[2] Vidal B, Polo V, Corral J L and Marti J 2003 *Elect. Lett.* **39** 547
[3] Vidal B, Piqueras M A and Martí J 2007 *Opt. Lett.* **32** 23
[4] Yu Y, Dong J J, Xu E M, X. Li, Zhou L N, Wang F and Zhang X L 2011 *IEEE J. Lightw. Technol.* **29** 3542
[5] Zhang Y, Zhang X L, Chen G J, Xu E M and Huang D X 2010 *Chin. Phys. Lett.* **27** 074207
[6] Xu E M, Zhang X L, Zhou L N, Zhang Y and Huang D X 2009 *Chin. Phys. Lett.* **26** 094208
[7] Rasras M S, Kun-Yii T, Gill D M, Chen Y K, White A E, Patel S S, Pomerene A, Carothers D, Beattie J, Beals M, Michel J and Kimerling L C 2009 *IEEE J. Lightw. Technol.* **27** 2105
[8] Chen J X, Wu Y, Hodiak J and Yu P K L 2003 *IEEE Photon. Technol. Lett.* **15** 284
[9] Chan E H W, Alameh K E and Minasian R A 2002 *IEEE J. Lightw. Technol.* **20** 1962
[10] Dong J J, Liu L, Gao G S, Yu Y, Zheng A L, Yang T and Zhang X L 2013 *IEEE Photon. J.* **5** 5500307
[11] Chan E H W and Minasian R A 2004 *Elect. Lett.* **40** 1375
[12] Zhang W, Williams J A R and Bennion I 1999 *Elect. Lett.* **35** 2133
[13] Zhu Y, Xu X J, Li Z Y, Zhou L, Han W H, Fan Z C, Yu Y D and Yu J Z 2010 *Chin. Phys. B* **19** 014219
[14] Alipour P, Eftekhar A A, Atabaki A H, Li Q, Yegnanarayanan S, Madsen C K and Adibi A 2011 *Opt. Express* **19** 15899
[15] Chen L, Sherwood-Droz N and Lipson M 2007 *Opt. Lett.* **32** 3361
[16] Zhang D, Xue F and Huang Y 2012 *IEEE Photon. Technol. Lett.* **24** 1502
[17] Abreu-Afonso J, Diez A, Cruz J L and Andres M V 2012 *IEEE Photon. Technol. Lett.* **24** 2129
[18] Lee M C M and Wu M C 2006 *Opt. Lett.* **31** 2444
[19] Soltani M, Yegnanarayanan S and Adibi A 2007 *Opt. Express* **15** 4694